國立交通大學

光電工程研究所

碩士論文

氧化矽阻障層對矽奈米結晶薄膜之影響

Effects of Silicon Oxide Barrier Layers on Silicon Nanocrystal Thin Films

研究生:蔡宜恒

指導教授:李柏璁 教授

中 華 民 國 九十九 年 八 月

氧化矽阻障層對矽奈米結晶薄膜之影響

研究生:蔡宜恒

指導教授:李柏璁 教授

國立交通大學光電工程研究所碩士班

摘　要

為了達到一個低成本高效率的太陽能電池，全矽堆疊式太陽能電池具有很大的潛力，藉由不同能隙的矽奈米晶體薄膜(例如: Si/SiO_2矽奈米晶體薄膜)堆疊於單晶矽太陽能電池可減少熱損耗的發生，以提高整體之效率。Si/SiO_2矽奈米晶體薄膜導性深受 SiO_2阻障層的影響，為了提升該矽奈米晶體薄膜導電性，我們在阻障層中加入一些缺陷，去創造額外的路徑以提供載子傳輸。我們利用拉曼光譜去分析該缺陷對結晶以及矽奈米晶體尺寸的影響，並利用 X 光繞射分析去對尺寸做進一步的驗證，接著使用光激發光譜去探討阻障層對於缺陷態的變化，最後再藉由電性的量測探討該矽奈米晶體薄膜傳輸機制。

Effects of Silicon Oxide Barrier Layers on Silicon Nanocrystal Thin Films

Student : Yi-Heng Tsai

Advisor : Prof. Po-Tsung Lee

Institute of Electro-optical,

National Chiao Tung University

Abstract

In order to achieve low cost and high efficiency solar cells, all silicon tandem solar cells made of Si nanocrystal (Si NC) thin films with different bandgaps (such as Si/SiO_2 Si NC thin films) stacking on crystalline Si solar cells are proposed. The solar cells can greatly reduce thermalization loss. However, Si/SiO_2 Si NC thin films exhibit low conductivity because of poor conductivity of SiO_2 barrier layers. In this thesis, we created additional transportation paths by increasing the defects of barrier layers. We studied effects of the defects on the crystallization and dimension of Si NC thin films by Raman spectra and XRD. In addition, we analyzed the influences of the defects on optical properties of Si NC thin films by PL spectra. Finally, we discussed a possible carrier transportation mechanism from electrical results.

Acknowledgements

首先，我想要感謝我的家人，除了對我求學路上的經濟援助以外，對於求學期間所遇到的困難與挫折，也不斷的給予我寶貴的意見，讓我在求學的路上不會感到孤獨，家人的支持與鼓勵也是我求學的動力來源。

研究所的生活雖然只有短短的兩年，但卻令我受益匪淺，雖然在研究過程中，不斷的遇到挫折以及失敗，但憑著不屈不撓的精神，以及實驗室的夥伴們對於實驗上的幫助，使得研究終於有所成果。因此我想特別感謝我的指導教授李柏璁老師，感謝老師在這兩年中對於我在實驗方面的指導，使得在研究過程中所遇到的難題得以解決，此外還要感謝與我一起奮鬥的實驗室夥伴，感謝又瑋、鈞隆、品佐、君源在我實驗忙不過來的時候出手相助，感謝贊文、資岳、明峯、光揚、家揚學長們在實驗過程中的寶貴意見，讓我可以更快找到成功的路，感謝金剛、文齡、立勛、紹平、雋威、品睿這群可愛的學弟妹們，讓我在實驗之餘帶給我歡樂，放鬆心情準備下次實驗的動力。最後再一次感謝實驗室所有的夥伴們，沒有妳們的幫忙，相信我的實驗不會這麼容易的有成果。

2010/09/06 于新竹 國立交通大學 交映樓 401 室

Content

List of Tables

List of Figures

Chapter 1 Introduction

1.1 Background

Energy crisis and environment protection are two main issues of the world nowadays. Fossil fuels are the main energy for human in the life. But fossil fuels are exhaustible and storage of fossil fuels is reducing drastically after industrialization. In addition, the average temperature of the earth is increasing due to the worse green house effect resulted from arising emission of green house gases such as CO_2 emissions after burning fossil fuels.

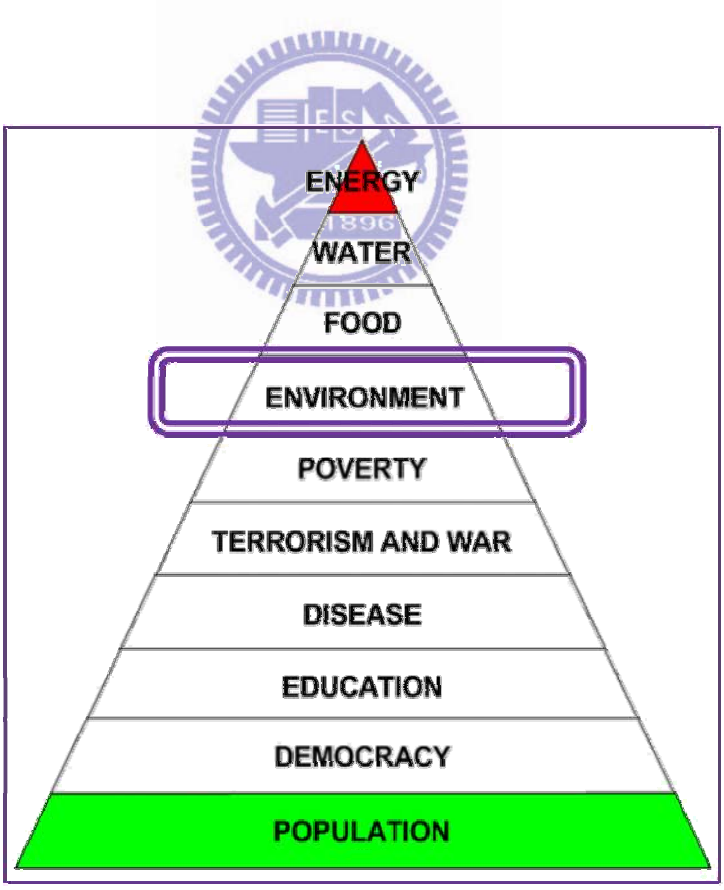

Fig. 1.1: Human`s top ten problems for next 50 years

Source: Richard Smalley, Rice University

The Fig. 1.1 shows the top ten problems for next fifty years. Energy and environment issues are top 1 problem and top 4 one of the world, respectively. It suggests that research and development of green energies (renewable and eco-friendly energies) is the front burner. There are lots of green energies (such as wind power, tide power, geothermal heat, solar energy) have been interested. Solar energy is much more potential green energy because of inexhaustible power from the sun and less limitation on the locations. It is promising to use solar energy to replace fossil fuels completely in the future with advancing technologies.

1.2 Solar cells

The first photovoltaic device (also called a solar cell) was created at Bell Laboratories in 1883 by Charles Fritts. However, solar cells had not drawn attention until the oil crises broke out in following decades. Recently, solar cells are greatly interested because of not only energy issues but also environmental issues such as increasing sea level resulted from the worse green house effect.

The illustration of structure and operation of solar cells are shown in Fig. 1.2

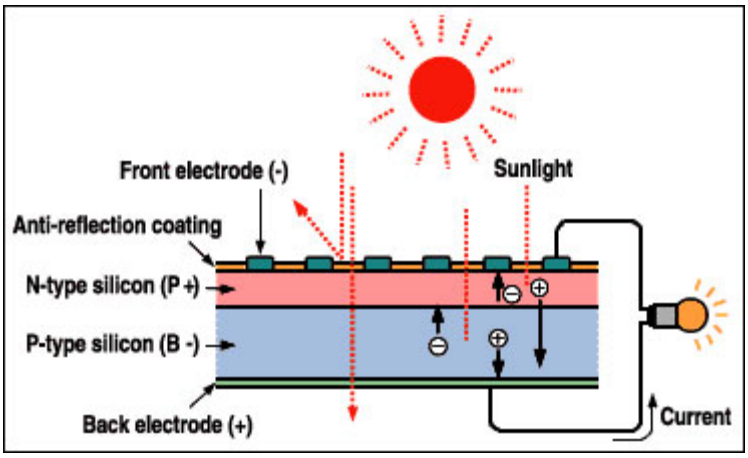

Fig. 1.2 : The illustration of structure and operation of solar cells

http://www.icembed.com/info-17526.htm

According to the efficiency as a function of cost, solar cells can be classified into three generations as the shown in Fig. 1.3.

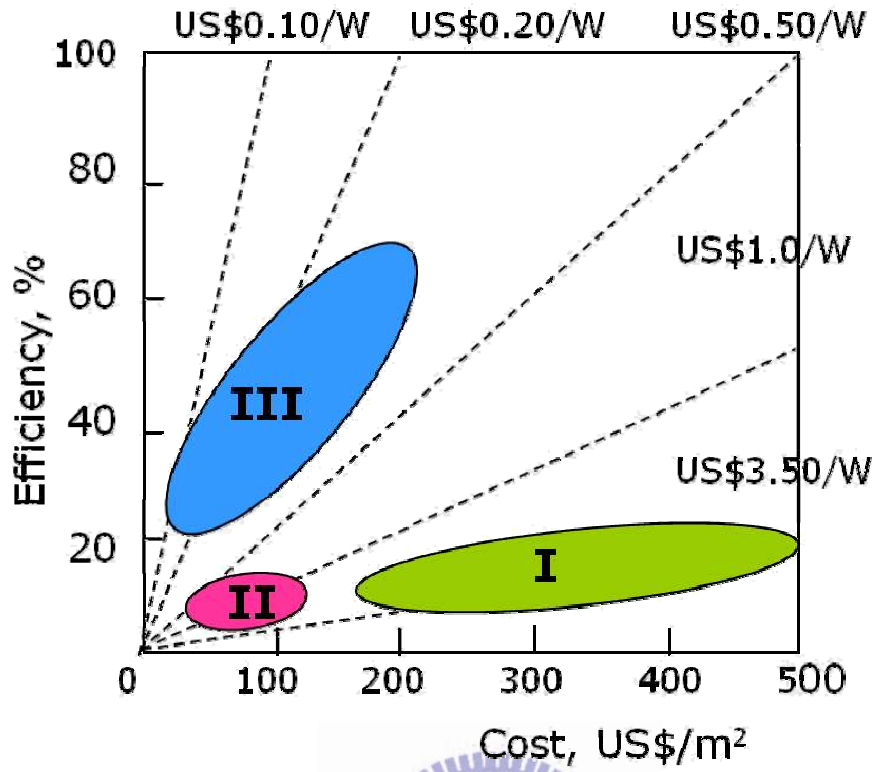

Fig. 1.3 Efficiency as a function of cost for first-, second- and third generation photovoltaic technology (wafer, thin films and advanced thin films respectively) **[1]**

First generation solar cells are silicon wafer based solar cells. The technology of first generation solar cells has matured and the solar cells dominate the market of solar panels because of their high efficiency. Although the solar cells perform high efficiency, the manufacturing cost also very high. For reducing the cost, second generation solar cells (that is, thin film solar cells such as amorphous silicon solar cell, and copper indium diselenide solar cells) has been developed. The cost of second generation is

quiet cheaper than that of first generation solar cells. On the other hand, the efficiency of second generation solar cells is less than that of first generation solar cells. Other main features of second generation solar cells is their flexibility and light-weight which makes lots of application innovations such as flexible solar panel. For achieving solar cells with high efficiency which is potential to be larger than efficiency limit of solar cells with single bandgap (31%) and low manufacturing cost, a wide range of promising solar innovations including polymer solar cells, nanocrystalline cells, and dye-sensitized solar cells (third generation solar cells) are being studied. Even if third generation solar cells are superior to the others, third generation solar cells are still in the research phase.

1.3 Silicon based tandem solar cells

1.3.1 Power Loss Paths

There are five power loss paths in standard single junction solar cell, including thermalization loss, junction loss, contact loss, recombination loss and non-absorption loss as shown in Fig. 1.4.

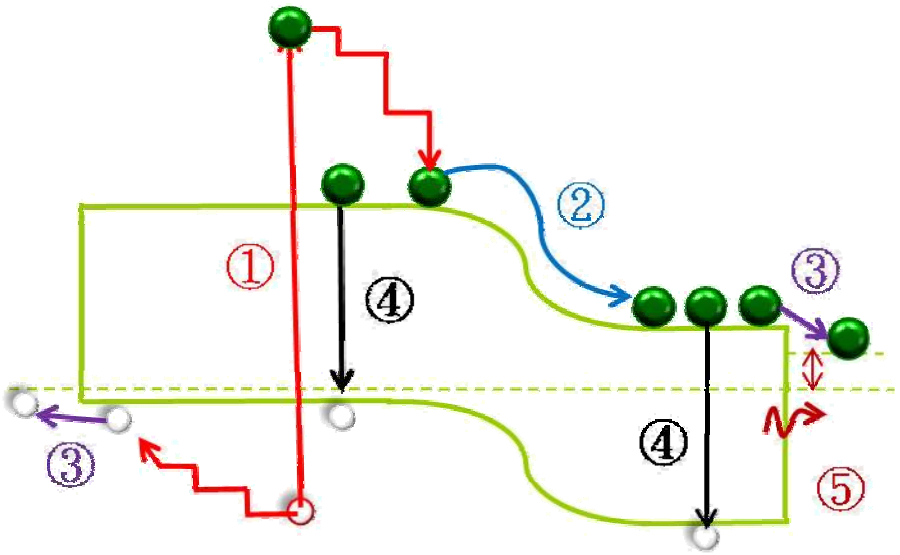

Fig. 1.4: Power loss paths in single band-gap solar cell

And there are two primary power loss paths in single band-gap photovoltaic cells: thermalization of photons with energy larger than the band gap and waste of photons with energy less than the band-gap [2]. Stacking materials with different energy band-gaps, collection of photo-excited carriers before thermalization, multiple carriers per photon via impact ionization, and energy-down conversion are potential approaches to tackle these two power loss problems. Tandem solar cell, stacking sub-cells from large band-gap to small band-gap in turn, is a much more promising structure to achieve a high energy conversion efficiency solar cell. Si nanocrystals (NCs) can be made very small, less than 7 nm in diameter, and they behave like quantum dots (QDs), e.g. band-gap control with nanocrystal size, very fast optical transition, and multiple carrier generation, owing to the three-dimensional quantum confinement of carriers [3]. Si NCs

embedded in dielectric matrices cascaded with silicon-based solar cells is one of the proposed solar cell structures to achieve super high energy conversion efficiency due to its flexibility in energy band-gap engineering.

1.3.2 Quantum Confine Effect

Behavior of particle waves confined in an infinite quantum well can be explained by three-dimensional time-independence Schrödinger's equation can be express by

$$-\frac{\hbar}{2m}\nabla^2\Psi(\vec{r})+V(r)\Psi(\vec{r})=E\Psi(\vec{r}) \qquad (1.1)$$

We can obtain that allowance energy states are discrete and they depend on width of the quantum well. The phenomenon is the quantum confinement effect. For particle-waves confined in nanoparticles covered in materials with finite barrier heights, similar energy states can be obtained, as expressed by eq. 1.2.

$$E_n=\frac{\hbar^2\pi^2}{2ma^2}n^2 \quad , \quad n^2=(n_x{}^2+n_y{}^2+n_z{}^2) \qquad (1.2)$$

where n_x, n_y, n_z are integers and equal to 1 for the ground state square box.

Discrete energy levels depend on the dimension of nanoparticles and barrier height between nanoparticles and materials which cover around them. Fig. 1.5 shows wave functions of different size of nanoparticles with a fixed barrier height and those of different barrier height with a fixed size of nanoparticles. As a result, we can control effective Eg by tuning the dimension of Si NC and changing materials of barrier layers.

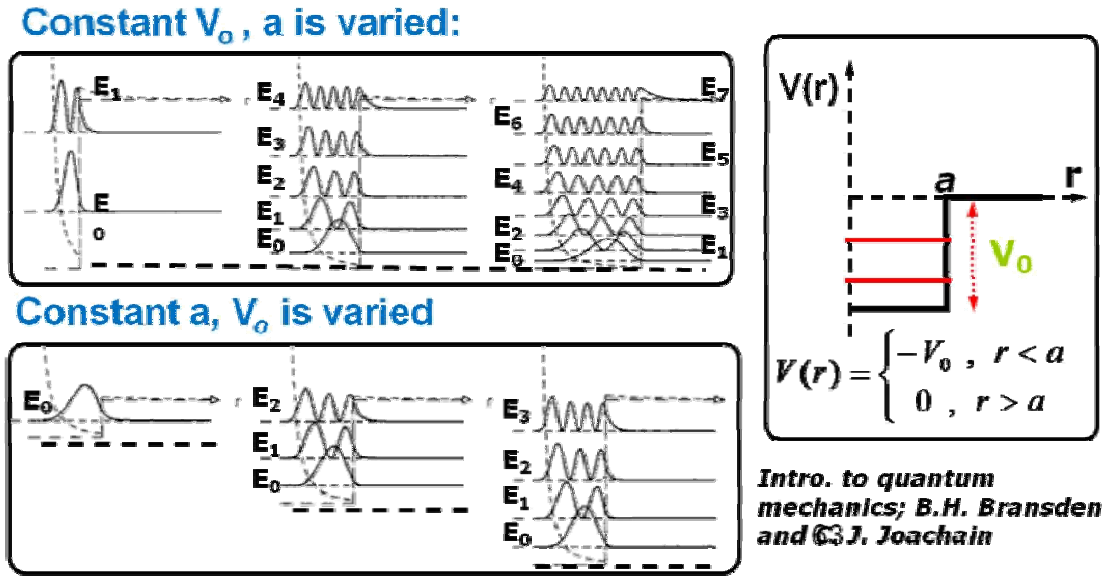

Fig. 1.5: 3-D time-independence Schrödinger's equation and boundary conditions.

1.3.3 Tandem solar cells using Si NC thin films

In order to achieve high efficiency low cost solar cell, the third generation solar cells have been studied. One of the promising candidates is tandem solar cell using Si NC thin films as shown in Fig. 1.6.

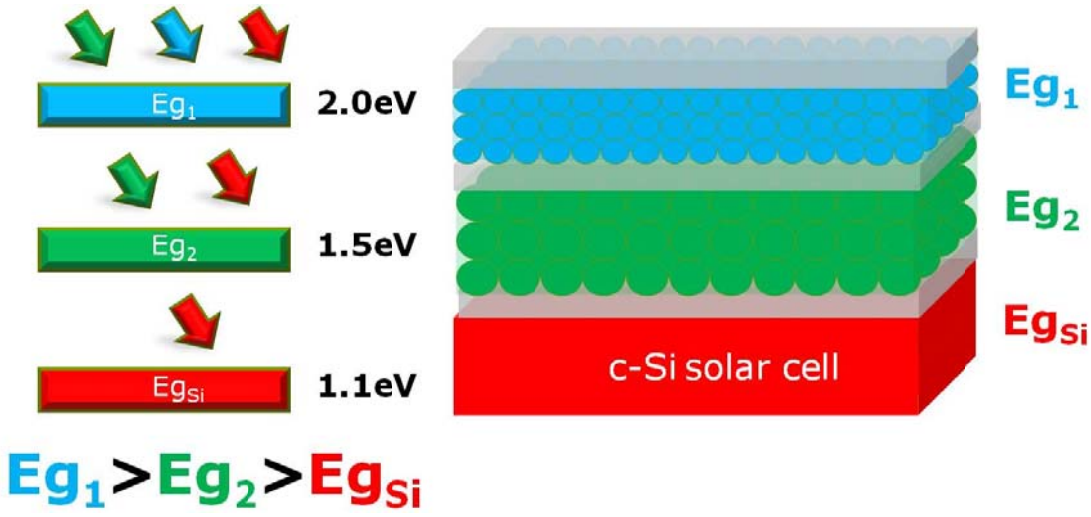

Fig. 1.6 : Schematic of Si-based tandem solar cell

Tandem solar cells using Si NC thin films stacking material with different energy bandgaps can utilize the wide solar spectrum more effectively. Table1.1 shows upper limits of conversion efficiency of solar cells calculated according to the number of optimal bandgap of active materials. Under one sun illumination, the maximum efficiency is 68.2% for solar cells with infinite bandgaps. Table1.2 shows the best efficiencies of a crystalline silicon solar cell (Eg = 1.1 eV) stacking with a Si NC thin film(s) whose bandgap is optimized.

Table 1.1 : Efficiency depends on different stack solar cell.

Junctions in solar cell	1 sun η	Max con. η
1 junction	31.0 %	40.8 %
2 junctions	42.9 %	55.7 %
3 junctions	49.3 %	63.8 %
∞ junction	68.2 %	86.8 %

Table 1.2 : Efficiency optimal bandgap depends on different stack solar cells.

Stack number (n)	Value of bandgap(eV)	η (%)
2	1.7	42.9
3	1.5, 2	49.3
4	0.6, 1.11, 1.69, 2.48	62.0
5	0.53, 0.95, 1.4, 1.93, 2.68	65.0
6	0.47, 0.84, 1.24, 1.66, 2.18, 2.93	67.3
7	0.47, 0.82, 1.19, 1.56, 2.0, 2.5, 3.21	68.9
8	0.44, 0.78, 1.09, 1.4, 1.74, 2.14, 2.65, 3.35	70.2

1.4 Paper Review

Silicon has a poor optical radiative efficiency because of its nature of indirect bandgap. Thus, rare research works on silicon optoelectronics has been published until strong photoluminescence from near infrared to ultraviolet in porous Si was observed, which is ascribed to the quantum confinement effect. In addition to porous Si, Si nanocrystals (NCs) embedded in dielectric mediums such as silicon dioxide have been also investigated due to the potential for optoelectronic applications such as photovoltaic devices.

Many fabrication methods of Si NCs embedded in dielectric mediums such as plasma-enhanced chemical vapor deposition (PECVD), [4] ion implantation [5] and sputtering [6] are proposed. Nae-Man Park et al. fabricated Si quantum embedded in Si nitride matrix by PECVD with SiH_4 and N_2 as reactant gas sources. [4] The properties

of Si quantum can be controlled by adjusting the flow of gas sources or different reactant gas sources. J. I. Wong et al. prepared their Si NC thin films by implanting Si ions into SiO_2 thin films. [5] First, the SiO_2 thin films were grown with O_2 and H_2 in high temperature furnace. Then Si ions were implanted with different dose and energy into the SiO_2 thin films. Finally, thermal annealing was carried out for NCs formation. Eun-Chel Cho et al. made their Si NC thin films by sputtering. [6] First, multiple alternative layers of amorphous Si rich oxide (SiO_x, $x<2$) and stoichiometric SiO_2 as presusor thin films were deposited by cosputtering with SiO_2 and Si targets and sputtering with a SiO_2 target, respectively. Then Si NC thin films were obtained after the precursor thin films annealing at high temperature such as 1100℃ for 1 hr. The dimension and density of Si NCs can be controlled by adjusting the thickness and Si content of amorphous Si rich oxide.

One of important applications of Si NC thin films is photovoltaic devices. Martin A. Green et.al, demonstrate that the efficiency of solar cells using Si NCs embedded in SiO_2 is up to 10%. [6] Although this is a big progress in solar cells using Si NC thin films, the efficiency is still far away the theoretical values predicted using detail balance limit. The poor performance can be attributed to large power loss in the solar cells such as poor carrier collection efficiency results from low conductivity of SiO_2.

Although defects in SiO_2 resulted from amorphous SiO_2 [7] can offer

transportation paths for carriers, the conductivity of Si NC thin films for photovoltaic devices is not high enough. In order to further reduce power loss from poor carrier collection efficiency, many results has been published. For Si/SiO_2 multilayer structures, carriers are easily blocked by in the direction perpendicular to the thin films because of higher barrier height. Conductivity can be enhanced effectively if the barrier height is reduced. Lateral contact was introduced to enhance the carrier transportation. [7] When carries transport parallel to the barrier, the effective barrier height will be lower than transport through the barrier layers. Hence, conductivity can be enhanced for the lateral contact. [8] B. Berghoff et al. proposed a Si/SiO_x multilayer structure to improve the conductivity. [9] Si NC thin films formed by annealing precursor thin films using a Si/SiOx structure leads to the precipitation of excess from SiO_x layers to Si layers. The morphology of SiO_x layers were changed after annealing, and he ultrathin SiO_2 layers formed. Thus the barrier height is reduced due to the thinner SiO_2 layers. Hence, conductivity can be enhanced due to the lower barrier height caused by thinner SiO_2 layers. In addition, the dopant concentration of Si NC thin films and barrier height between Si NCs and barrier layers also affect the conductivity of Si NC thin films. X. J. Hao et al. made boron-doped Si NC thin films by RF co-sputtering with Si, SiO_2 and boron targets. The boron concentration was controlled by adjusting the power applied to the boron target. It was demonstrated that the resistivity of Si NC thin films decreases

by increasing the power applied to the boron target. In other words, the resistivity decreases by increasing the boron concentration of Si NC thin films. [10] Gavin Conibeer et al. fabricated Si NCs embedded in Si_3N_4 to increase the conductivity because of lower barrier compared to SiO_2. [11]

1.5 Motivation

In this work, we added additional silicon in barrier layers (SiO_2 layer) to form defect states. The defect states in barrier layers can offer additional transportation sites for photo-generated carriers, and thus increase the conductivity of the Si nanocrystal thin films. Therefore, it is expected that the conversion efficiency of the solar cell can be enhanced effectively due to the enhancement of thin films conductivity.

The main purpose of this thesis is to investigate the characterization and electrical properties after increasing Si content in barrier layers.

Chapter 2 Fabrication of Si Nanocrystal thin film

In this chapter, we introduce all the fabrication process of our samples. The process flow is shown in Fig. 2.1.

Fig. 2.1 : Process flow of Si nanocrystal thin film

2.1 Substrate Clean

The beginning step as shown in Fig. 2.1 is substrate clean. Si wafers will be cleaned by RCA clean shown in Table 2.1. The main purpose of RCA clean is to remove the particle and native oxide on the wafers. And in the cleaning process of quartz, we use aceton and deionized water with ultrasonic cleaner to remove the organic contaminates on the quartz.

Table 2.1 : RCA clean process of substrate

Preliminary RCA clean	
Step 1	5 min in DI water rinse
Step 2	10~15 min in (3 : 1) proportion H_2SO_4 / H_2O_2
Step 3	5 min in DI water rinse
Step 4	10~15 sec in (1 : 100) proportion HF/ H_2O
Step 5	5 min in DI water rinse

2.2 Precusor Thin Film Deposition

Precusor thin films of Si NC thin films compose of superlattice structures using two different materials such as Si/SiO_2. All precursor thin films were deposited by radio frequency (RF) magnetron sputtering as shown in Fig. 2.2. SiO_2 target and P type Si target with the resistivity about 0.005 Ωcm ~ 0.02 Ωcm were adopted. Silicon rich silicon oxide thin films were obtained using cosputtering of Si and SiO_2 targets. We modified the power of targets to control the composition of depositing thin films and the duration of shutters to tune the thickness of the each thin film.

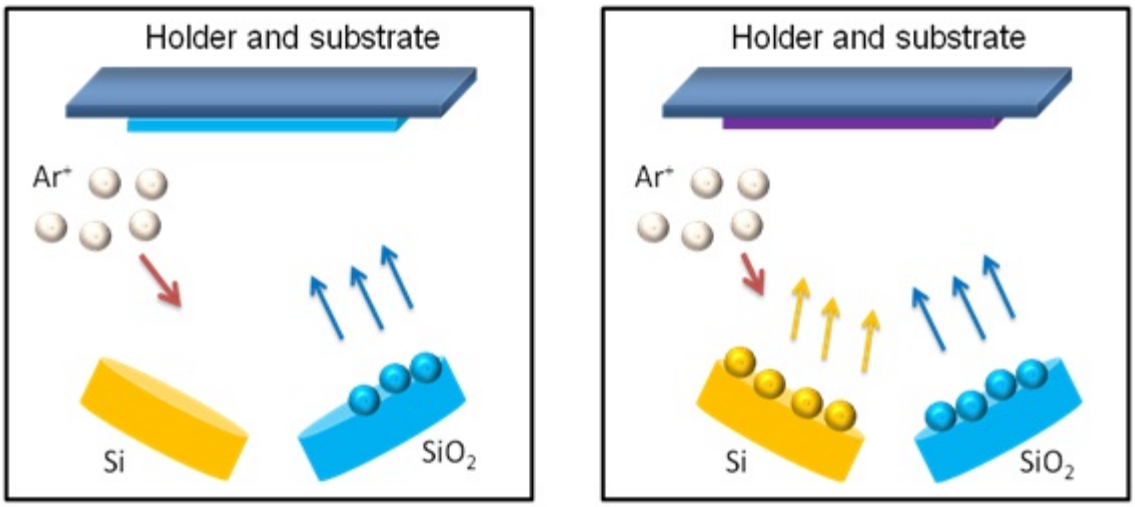

Fig. 2.2 : Operation of magnetron sputtering and co-sputtering.

Fig. 2.3 shows the multilayer structures of presusor thin films. For active layers, we deposited pure Si layer and high silicon rich oxide (HSRO) layer with the Si concentration about 82.3%, and for barrier layers, we deposited pure SiO_2 layer and low silicon rich oxide (LSRO) with the Si concentration about 32.8%. The thickness of active layers and that of barrier layers are 4 nm and 2 nm, respectively.

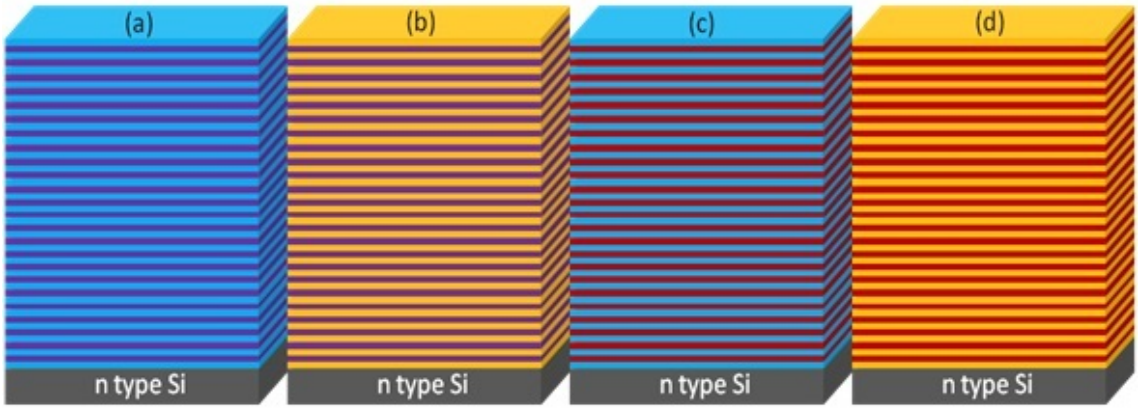

Fig. 2.3 : Precusor thin films (a)Si/SiO_2 (b) Si/LSRO (c) HSRO/SiO_2 (d) HSRO/LSRO multilayer with 4 nm (active)/2 nm (barrier) for each pair and total thickness is 146 nm (24pairs)

2.3 Formation of Si NC Thin Films

For the Si/SiO_2 and HSRO/SiO_2 multilayer structures as shown in Fig. 2.4(a), Si will precipitate in active layer after high temperature thermal annealing process due to phase separation of Si and SiO_2 according to the following equation:

$$SiO_x \xrightarrow{annealing} \frac{x}{2}SiO_2 + \left(1-\frac{x}{2}\right)Si \qquad (2.1)$$

Here we annealed all sample at 1100 for 1 hr in quartz furnace to form Si NC thin films.

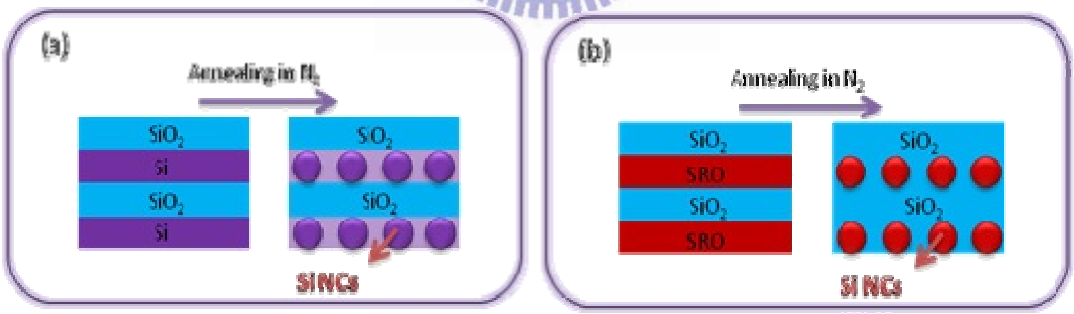

Fig. 2.4 : Schematic of as-deposited (a)Si/SiO_2 (b) HSRO/SiO_2 multilayer structure

2.4 Remove Thermal Oxide after Annealing Process

After annealing process, a thick thermal oxide layer was formed on the top and bottom of samples due to residual oxygen in the furnace. The thermal oxide layers make an influence on the collection efficiency of photo-generated carriers. In order to reduce the influence of the thermal oxide layers, we removed top side oxide layers by reactive ion etching (RIE) and bottom side oxide layers by buffered oxide etch (BOE).

2.5 Metal Deposition

Finally, contact electrodes were deposited on samples for the electrical properties measurement. In our work, the Si NC thin film is P type due to the Si target with B doping and the substrate is n type. Therefore, we deposited Au on the top of samples and Al on the bottom of samples in order to reduce the influence of contact.

Chapter 3 Characterization of Si NC Thin Films

In order to understand the characteristics of our Si NC thin films, measuring micro-Raman spectra, X-ray diffraction (XRD) pattern and photoluminescence (PL) spectra of our Si NC thin films were measured. Micro-Raman spectra can offer crystalinity and dimension of Si NC thin films. We can obtain crystalization phases and dimension of Si NC thin films. From PL spectra, we can analyze quantum confined related radiative signals and other radiative defect states.

3.1 Analysis of Si NC thin films by High Resolution Confocal-Raman Microcscope

3.1.1 Fundamental of Confocal Raman Microscope

Confocal-Raman Microscope is a powerful characterization technique for various semiconductor and insulator materials. It's based on the Raman effect, which is the inelastic scattering of photons and molecules [12].

We analyzed our samples by high resolution confocal Raman microscope (Lab RAM HR Raman Microscope), and we used a diode pumped solid state (DPSS) laser with 488nm wavelength. The illuminated spot size is about 10 um in diameter and the power of the laser is about 7mW. Si substrate was used to calibrate the crystalline signal

on 520 cm^{-1} before measuring Raman spectra of our samples.

Generally three peaks can be detected in Si NC thin films, including a amorphous mode (480 cm^{-1},), a transition mode (500~509 cm^{-1}) and a crystallization mode (510~519 cm^{-1}). In addition, Peak shift away from 520cm^{-1} and full width at half maximum (FHWM) of Raman spectra can be utilized to roughly estimate dimension of Si NC thin films because of the phonon confinement effect, as show in Fig. 3.1 [13]. Phonon confinement model can be expressed as follow equation :

$$L(w,D) \propto \int \frac{\sin[(qD/a)\pi]^2}{[1-(qD/a)^2]^2} \frac{dq}{[w_{opt}(q)-w]^2+(\Gamma/2)} \quad (3.1)$$

were L(w,D) is the lineshape of phonons confined to a hard sphere of diameter D, a is lattice parameter of Si, and Γ is the damping parameter [14].

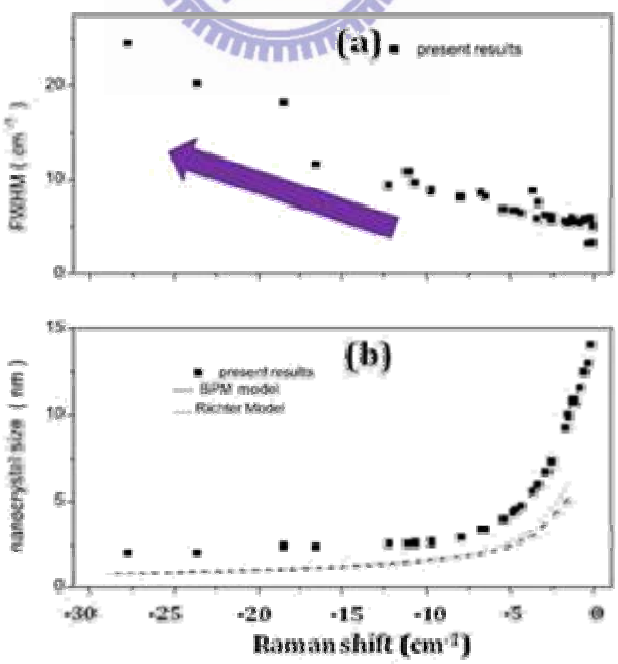

Fig. 3.1 : FWHM and size of the Raman peaks against the corresponding Raman shift [13]

3.1.2 Experimental Results and Discussions

Figure 3.2 shows the Raman spectra of Si NC thin films with different conditions, including Si/SiO_2, Si/LSRO, $HSRO/SiO_2$ and HSRO/LSRO multilayer structures with 24 pairs. Crystallization signals can be observed in all four structures. Peak positions, and FWHM of the Si NC thin films are listed in Table 3.1.and intensity by a curve fitting method.

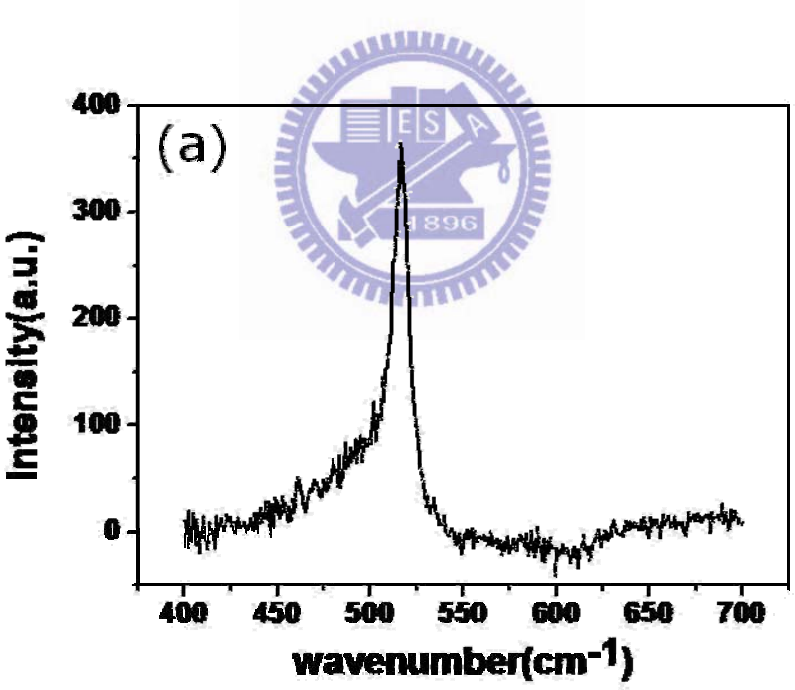

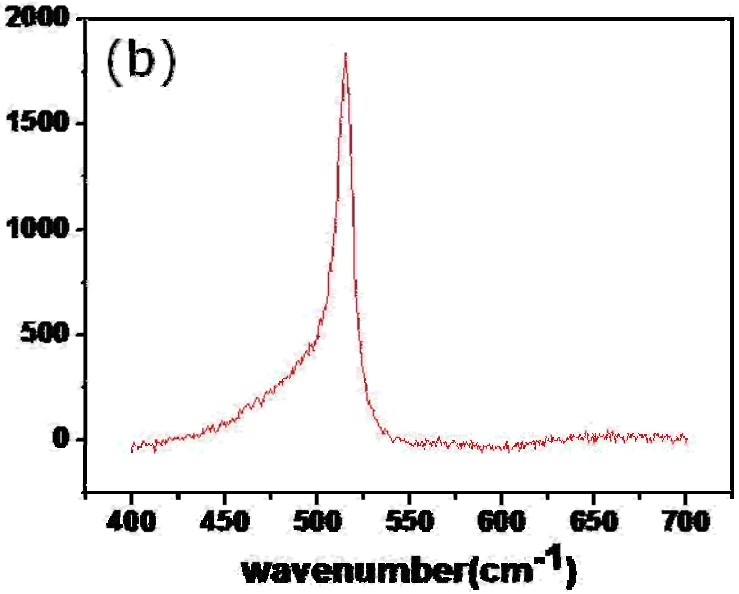
(b)
2000
1500
1000
500
0
400
450
500
550
600
650
700
wavenumber(cm-1)

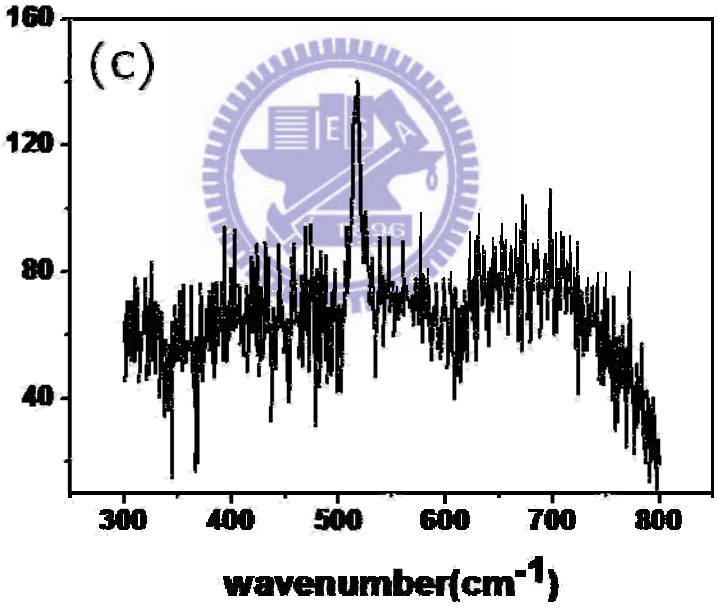
(c)
160
120
80
40
300
400
500
600
700
800
wavenumber(cm-1)

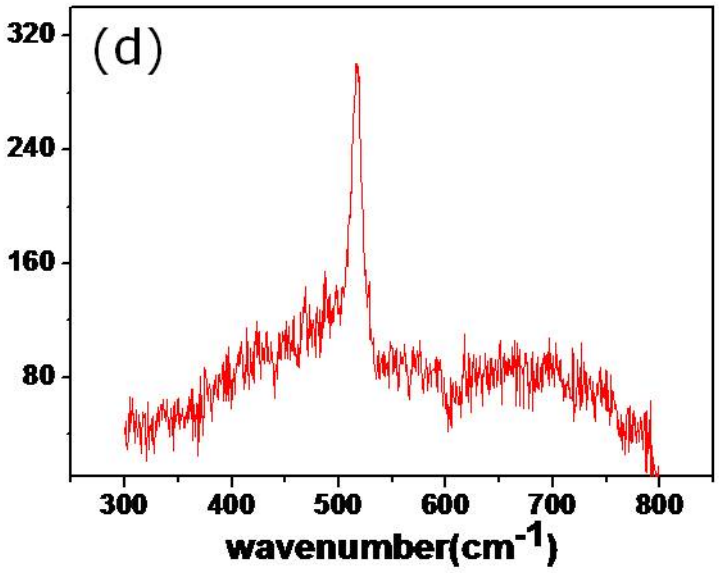

Fig. 3.2 : 24 pairs multilayer structure of (a) Si/SiO_2 (b) Si/LSRO (c) $HSRO/SiO_2$ (d) HSRO/LSRO after high temperature annealing process.

Table 3.1 : List of Raman spectra with different multilayer structure.

	Position(cm^{-1})	FWHM(cm^{-1})	Intensity(a.u.)
Si/SiO_2	516.83	9.03	247.95
Si/LSRO	515.15	8.4	1198.05
$HSRO/SiO_2$	517.59	13.27	66.31
HSRO/LSRO	516.51	12.77	180.56

It is obvious that the FHWM of Raman peaks decrease with increasing Si content

in barrier layers. It indicates dimension of NC can enlarge when Si content of barrier layers is increased. By comparing the measured FWHM and that calculated shown in Fig. 3.1, we can roughly obtained the dimension of our Si NC thin films. The dimension of both Si/SiO_2 and Si/LSRO multilayer structures is about 4~6 nm and that of HSRO/SiO_2 and HSRO/LSRO multilayer structures is about 2.5 nm. For multilayer structures with LSRO barrier layers, the estimated dimension of NC is larger than that of multilayer structures with SiO_2 barrier layers. The enlargement of the dimension can attribute to release of stress and/or increase of Si content in Si NC thin films. However, using peak position to estimate the dimension of our Si NC thin films shows a contrary manner because of a stress effect resulted from a thermal extension difference between Si and SiO_2. The stress effect cab be expressed as a follow equation :

$$w = w_0 + \Delta w = w_0 + \left(\frac{1.88\text{cm}^{-1}}{\text{GPa}}\right) \times P \qquad (3.2)$$

where P in GPa and w in cm^{-1}. Although peak positions are not suitable to estimate the dimension of Si NC thin films, we can observe that peak positions of multilayer structures with LSRO barrier layers are closer to those calculated using the phonon confinement effect because of the release of stress.

3.2 Analysis of Si NC thin films by X-Ray Diffraction

3.2.1 Fundamental of XRD Analysis

XRD is a nondestructive technique for structural characterization of crystalline materials. In XRD, an X-ray beam with a 1.54 Å wavelength is incident onto samples and is diffracted by the plane of atoms of samples. Diffraction peaks can be observed if there are constructive interferences generated. The condition for constructive interferences is given by the Bragg 's law :

$$\lambda = 2d\sin\theta \tag{3.3}$$

where d is the spacing between atomic planes, λ is the X-ray wavelength and θ is the angle between atomic planes and the incident beam. [15] In addition to crystallization phases, we can also estimate the dimension of NC according to the Scherrer formula expressed as a follow equation:

$$L = \frac{k\lambda}{\Delta 2\theta(\text{rad}).\cos\theta} \tag{3.4}$$

where λ is the X-ray wavelength, 2θ is the Bragg diffraction angle, k is the constant close to 0.9 and $\Delta 2\theta$ is the integral breadth of the Bragg peak which can be expressed :

$$\text{breadth} = \frac{\text{FWHM}}{\eta\frac{2}{\pi}+(1-\eta)\frac{2\sqrt{\ln 2}}{\pi}} \tag{3.5}$$

where η is the number adopted as 0.5. [16]

3.2.2 Experimental Results and Discussions

As shown in Fig. 3.3, it is obvious that two peaks are detected from 20 degree to 70 degree in a 2θ mode scan. The peak position around 56 degree is the signal of substrate. And the other peak (28.3 degree) is the signal of Si (111). In order to estimate the dimension of Si NC, fine scans of all our sample were also recorded shown in the insets of Fig. 3.3. The dimension is 4.9 nm, 5.8 nm and 2.8nm for Si/SiO_2, Si/LSRO and HSRO/LSRO, respectively, which are estimated by the Scherrer formula. All values are consistent with those estimated using Raman spectra.

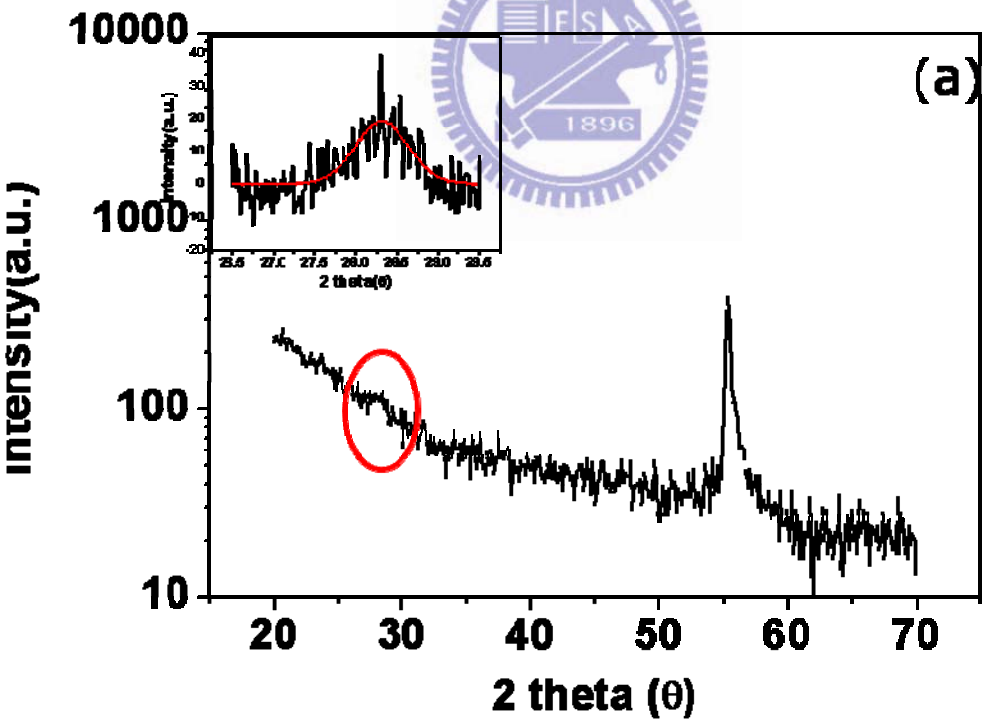

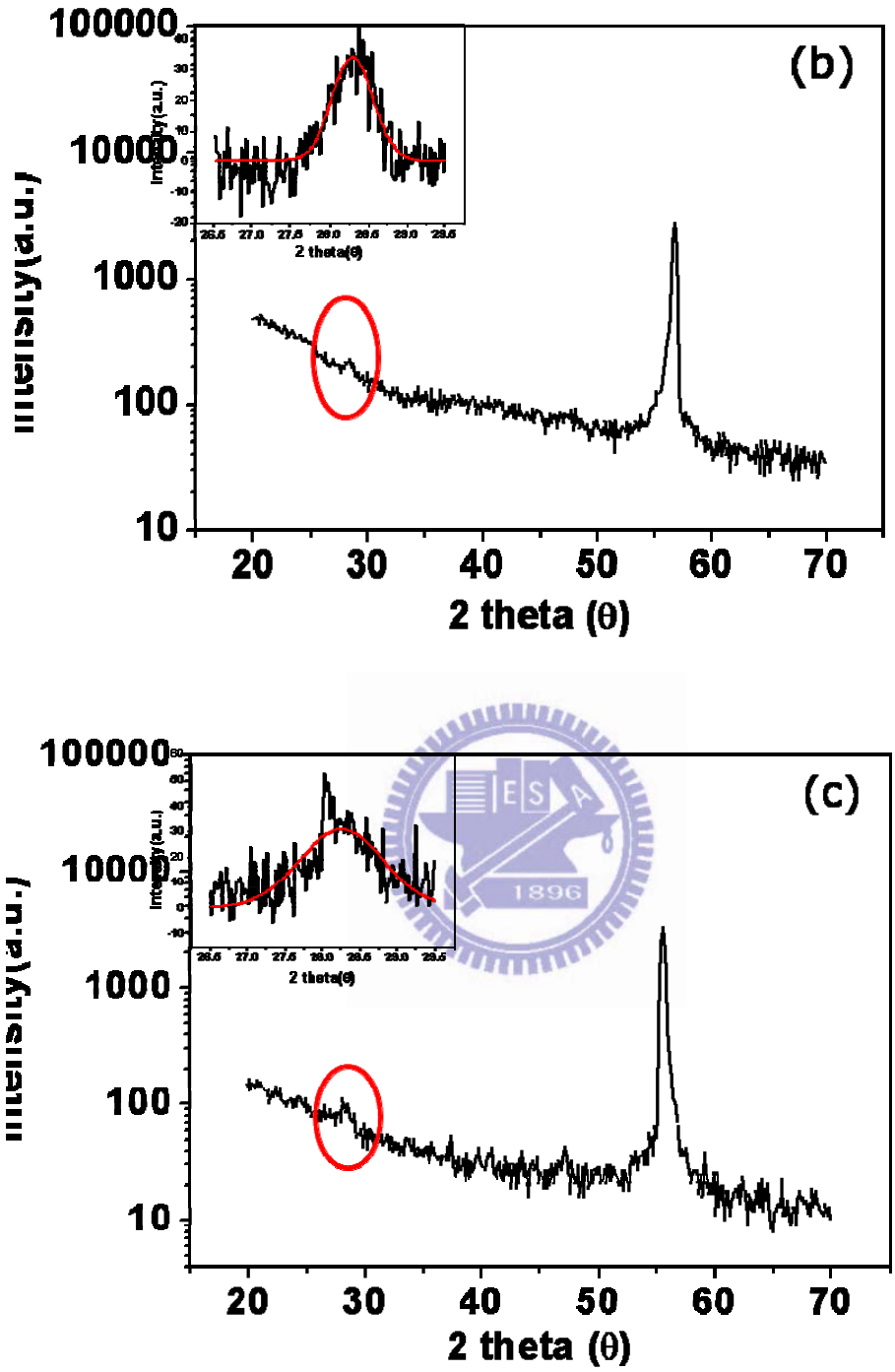

Fig. 3.3 : XRD analysis for (a) Si/SiO_2 (b) $HSRO/SiO_2$ (c) HSRO/LSRO multilayer with 24 pairs. The inset is precise scanning around 28.3 degree which is the signal of Si (1 1 1).

3.3 Analysis of Si NC thin films by PL Spectroscopy

3.3.1 Fundamental of PL Spectroscopy

PL spectroscopy is a contactless, nondestructive method of measuring the electronic structures of materials. When light is incident onto samples, where it is absorbed and imparts excess energy into the materials. The excess energy can be dissipated by the samples through the emission of light, or luminescence. We can realize the information of various important material properties from the emission of the light.

The instrument to measure PL spectroscopy of Si NC thin films is Lab RAM HR Raman Microscope. We also use a laser on diode pumped solid state (DPSS) with a 488nm wavelength. The illuminated spot size is about 10 um in diameter and the power of laser is about 7mW. Si substrate is used to calibrate the laser signal at 488 nm before measuring PL spectroscopy. All PL spectra are measured at room temperature (RT).

3.3.2 Experimental Results and Discussions

Figure 3.4 shows the PL spectra of our Si NC thin films. It is obvious that wide-ranged PL spectra are obtained. In other words, samples are probably with poor size distribution. However, the room RT-PL spectra of our Si NCs thin films are not only related to three-dimensional quantum confinement effect [17] but are determined by surface/interface-related defects, surface/interface passivation, [18] oxidation effects

[19] as well. For this reason, we decomposed the RT-PL spectra of our Si NCs thin films into three parts: defect states caused by LSRO barrier layers, quantum confinement effect and interface states. The peak position less than 700 nm is ascribed to defect states introduced by LSRO barrier layers and/or other defect states such as oxygen vacancy states. The peaks located at a range from 750 nm to 800 and at a range from 850 nm to 950 nm are probably because of the quantum confinement effect of Si NCs thin films and the radiative recombination of the interfacial defect states between Si NCs and the SiO_2 matrix. [20]

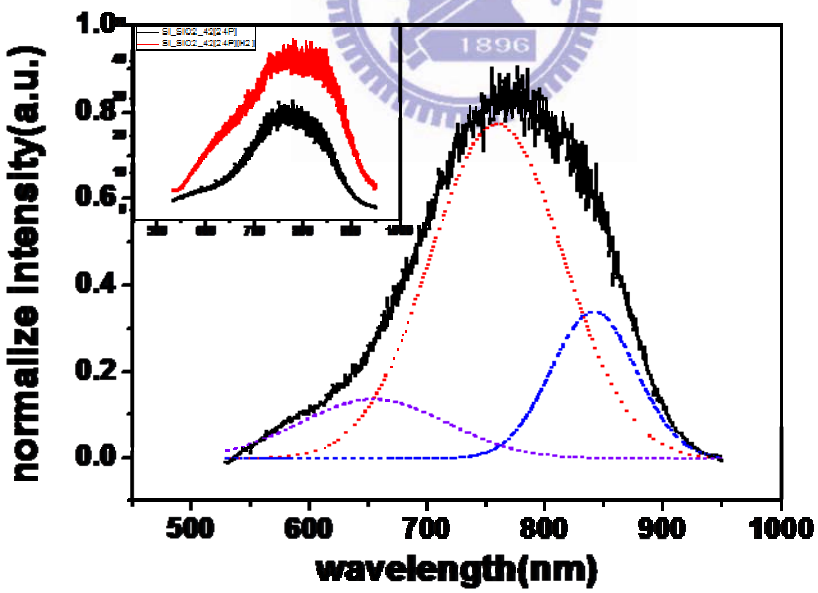

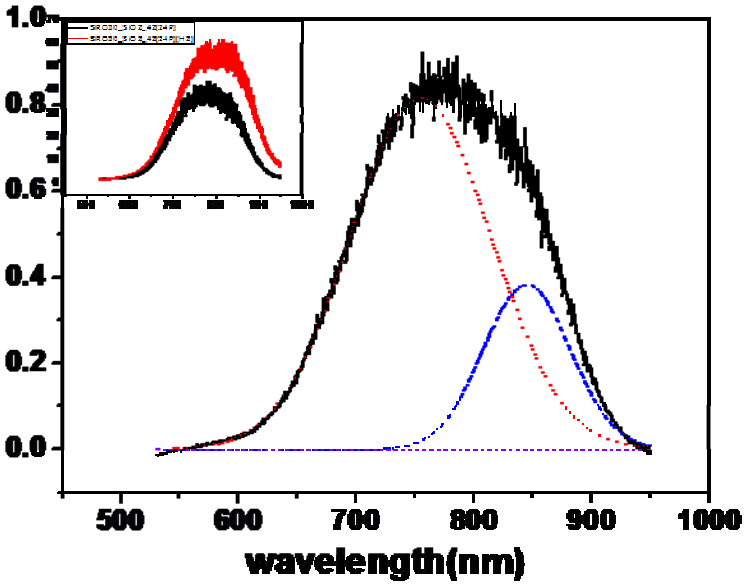
1.0
0.8
0.6
0.4
0.2
0.0
500
600
700
800
900
1000
wavelength(nm)

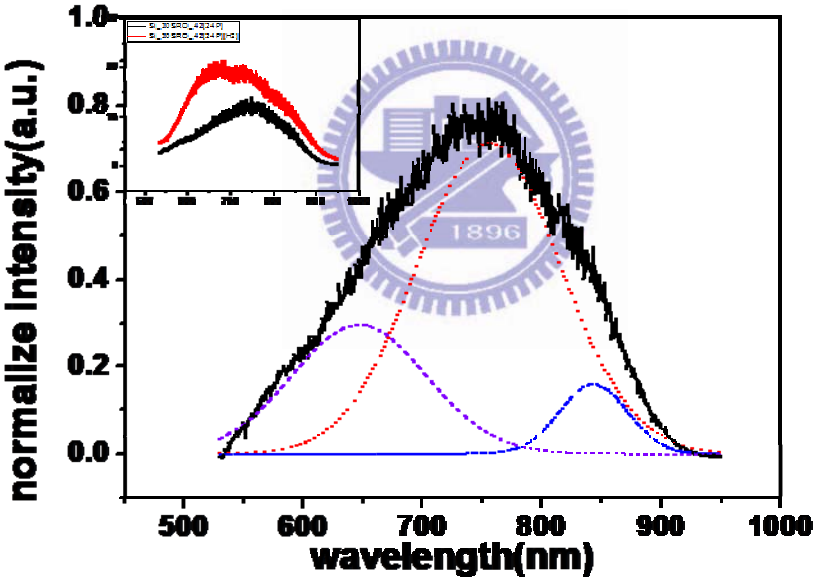
normallze Intenslty(a.u.)
1.0
0.8
0.6
0.4
0.2
0.0
500
600
700
800
900
1000
wavelength(nm)

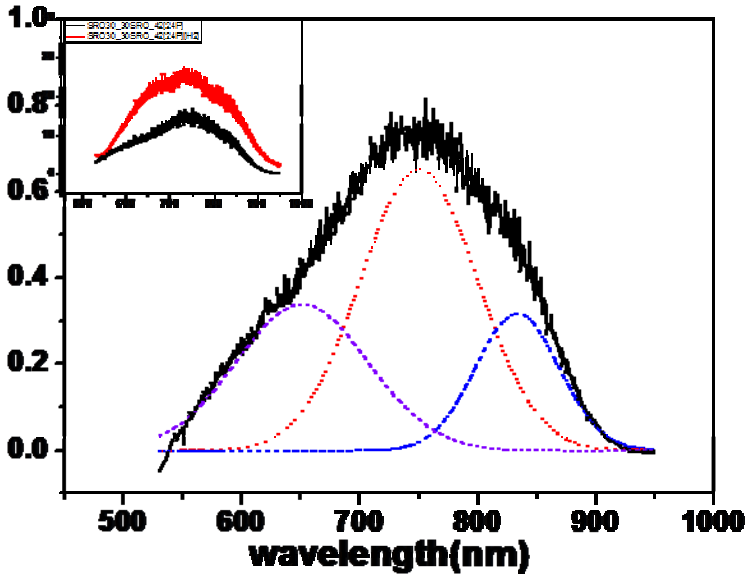

Fig. 3.4 : 24 pairs multilayer structure of (a) Si/SiO_2 (b) Si/LSRO (c) $HSRO/SiO_2$ (d) HSRO/LSRO after high temperature annealing process. The inset is the comparison between PL with and without H_2 passivation. The red line is with H_2 passivation and black line is not.

Non-radiative defects can quench the recombination of excitons and thus reduce the intensity of the PL spectra and /or eliminate some PL signals. To reduce the influence of non-radiative defects, we also measure the PL after H_2 passivation. From the inset of Fig. 3.4, there is an apparent enhancement in the PL spectra owing to the decrease of the non-radiative defects. Eventually, we list the peak position, FWHM and intensity of our Si NC thin films as shown in Table 3.2. We can observe that the intensity of PL peak less than 700nm of Si NC thin films with LSRO barrier layers is

larger that of Si NC thin films with SiO_2 barrier layers. No PL peak less than 700nm is obtained in Si NC thin films using a HSRO/SiO_2 multilayer structure. That is, PL peak less than 700nm attribute to defect states caused by LSRO barrier layers. However, PL peak less than 700nm is also observed in Si NC thin films using a Si/SiO_2 multilayer structure. The PL peak is probably resulted from the smaller Si NCs, a transition region between Si and SiO_2, or similar defect states as observed in Si NC thin films using a HSRO/SiO_2 multilayer structure. Although the origin of PL peak less than 700nm is not well understood, it can be enhanced and/or generated in the Si NC thin films with LSRO barrier layers. Moreover, it is expected that the defect states can create additional transportation paths for photo-generated carriers, and thus increase the conductivity of Si NC thin films.

Table 3.2 : Defect states of RT-PL spectra of with different multilayer structure.

	H_2 passivation	Position(nm)	FWHM(nm)	Intensity(a.u.)
Si/SiO_2	no	654.36	148.57	0.13
	yes	648.32	118.27	0.22
Si/LSRO	no	646.82	133.4	0.26
	yes	653.35	118.12	0.49
HSRO/SiO_2	no	NA	NA	NA
	yes	NA	NA	NA
HSRO/LSRO	no	651.34	131.89	0.3
	yes	651.84	112.49	0.36

Chapter 4 Electrical Properties of Si NC Thin Films

In this chapter, we focus on electrical properties of our Si NC thin films. We deposited Au on P type thin films and Al on N type Si substrate for ohmic contact. Current-voltage (I-V) curves of Si NC thin films are analyzed by HP 4156 semiconductor parameter analyzer. Photocurrent of Si NC thin films is measured under illumination with a halogens lamp (1500 lux).

4.1 Experiment Result and Discussions

As shown in Fig. 4.1, conductivity of Si NC thin films using Si/SiO_2 and $HSRO/SiO_2$ multilayer structures is very low, and their photocurrents are also not distinct from currents without illumination. In other words, Si NC thin films using Si/SiO_2 and $HSRO/SiO_2$ multilayer structures have poor photovoltaic properties because of low conductivity of SiO_2 barrier layers. On the contrary, Si NC thin films using Si/LSRO and HSRO/LSRO multilayer structures not only show higher current without illumination but also perform better photovoltaic properties. This can be ascribed to the effect of LSRO barrier layers which reduce stress to enlarge Si NC, thin the thickness of SiO_2 barrier layers, and provide additional transportation paths for carriers.

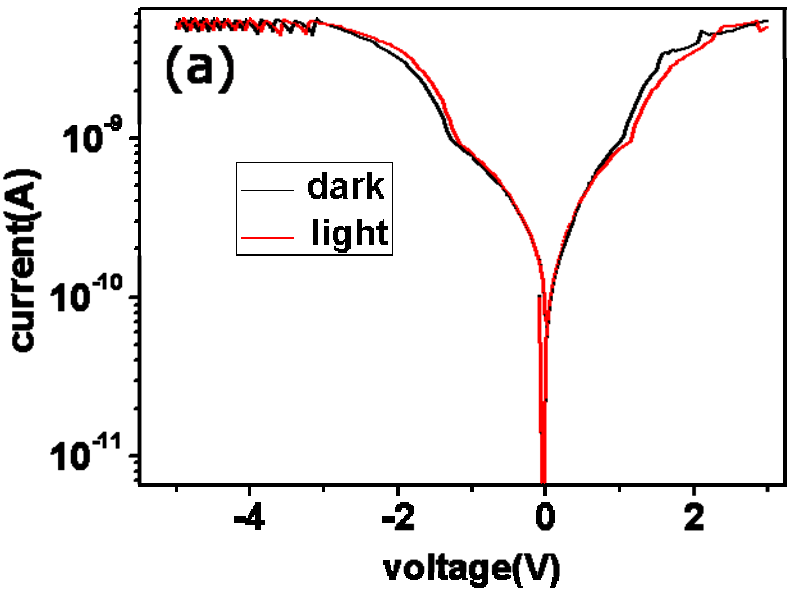
(a)
dark
light
current(A)
10^-9
10^-10
10^-11
-4
-2
0
2
voltage(V)

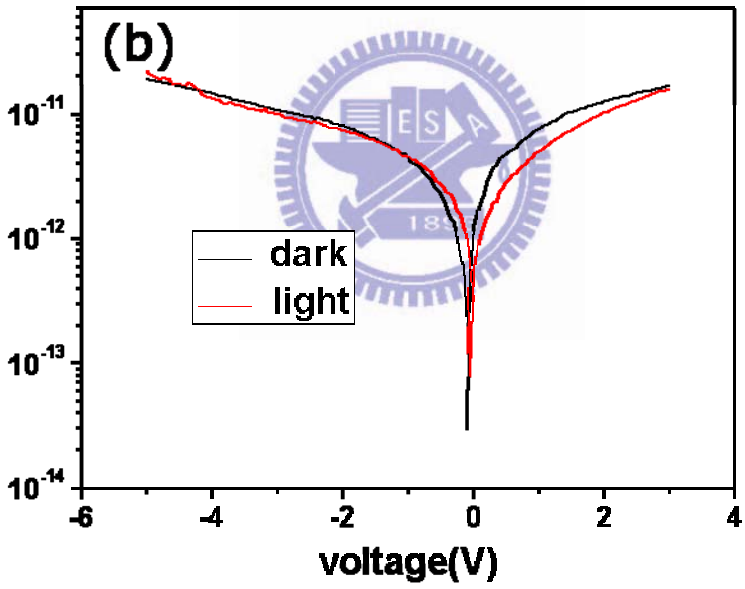
(b)
dark
light
10^-11
10^-12
10^-13
10^-14
-6
-4
-2
0
2
4
voltage(V)

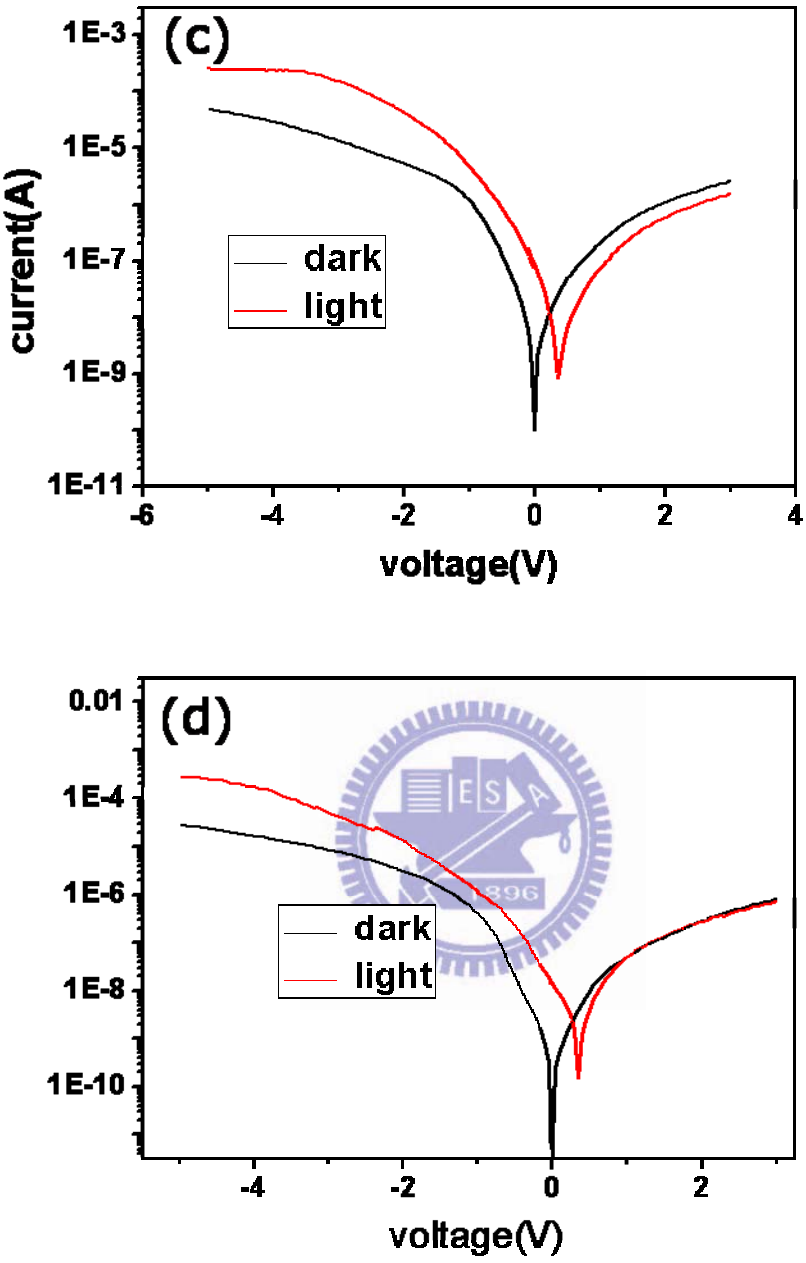

Fig. 4.1 : I-V characteristic for (a) Si/SiO_2 (b) $HSRO/SiO_2$ (c) Si/LSRO (d) HSRO/LSRO 24pairs multilayer structures.

Although the conductivity of Si NC thin films with LSRO barrier layers is largely enhanced, the electrical properties are still poor because of poor carrier collection

efficiency resulted from thicker SiO_2 barrier layers. Figure 4.2 shows I-V curves of a 12 pairs HSRO/SiO_2 multilayer structure and those of a 12 pairs HSRO/LSRO multilayer structure. Comparing with Si NC thin films using 24 pairs multilayer structures, the conductivity of Si NC thin films can be further improved after reducing the pairs of multilayer. Moreover, we find that the Si NC thin films composed of 12 pairs multilayer structures have a better photovoltaic effect. But there is no much more improvement if we reduce the pairs of multilayer structures less than 12 pairs. Therefore, it suggests that there is an optimal pair numbers of our multilayer structures.

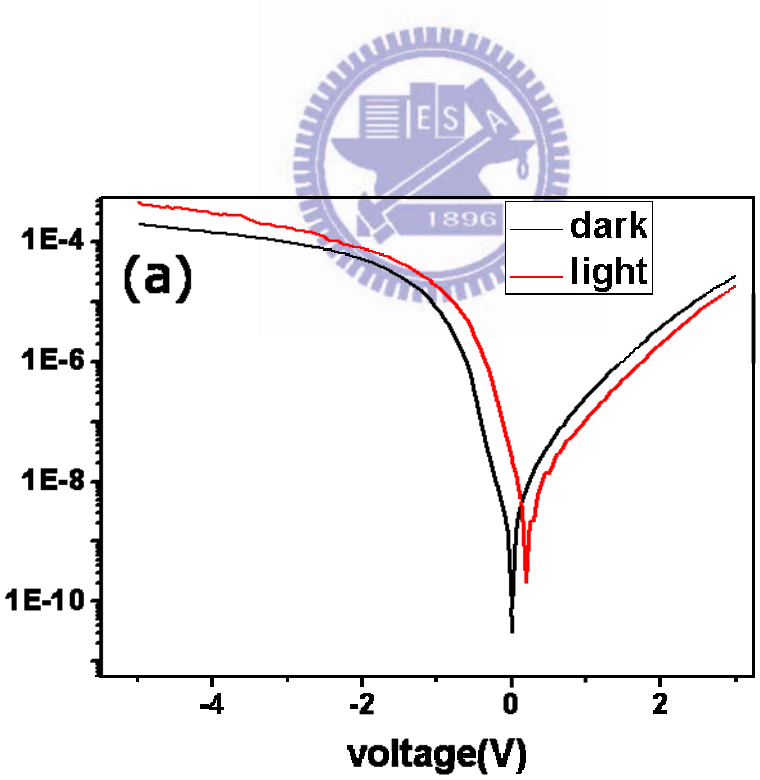

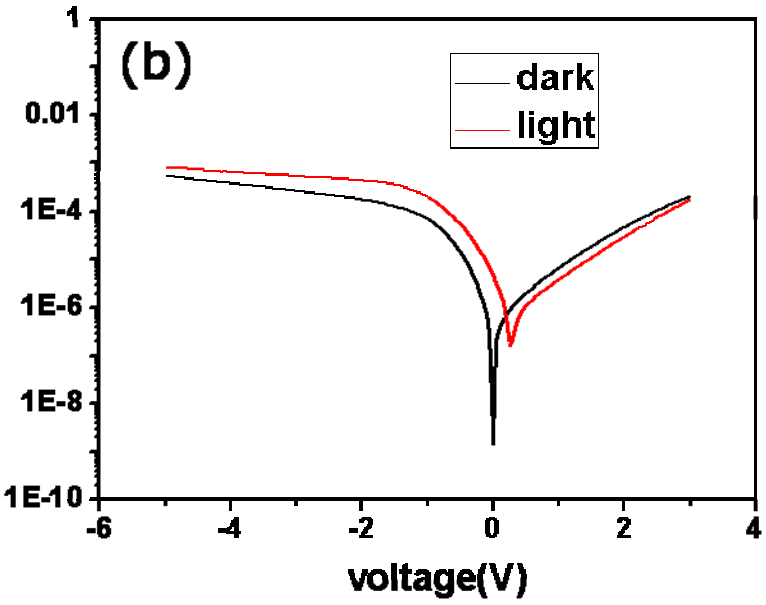

Fig. 4.2 : I-V characteristic for (a) HSRO/SiO_2 (b) HSRO/LSRO 12pairs multilayer structures without H_2 passivation.

4.2 Carrier Transport Mechanism of Si NC Thin Films

Many carrier transport models including Schottky emission, Fowler-Nordheim tunneling and Poole-Frenkel emission [22] are explained the transportation mechanism of Si NC thin films. Fig. 4.3 shows the curve fitting results of our Si NC thin films composed of Si/LSRO and HSRO/LSRO multilayer structures with Poole-Frenkel emission model according to the equation (4.1)

$$I/V = C\exp[-q/kT(\Phi - (qV/\pi\varepsilon l)^{1/2})] \quad (4.1)$$

where ε is dielectric constant, q is electronic charge, V is applied voltage, Φ is ionization energy of the traps, T is temperature, C is constant and k is Boltzmann

constant. As we can see, the I-V curves of two Si NC thin films well fit the transport model.

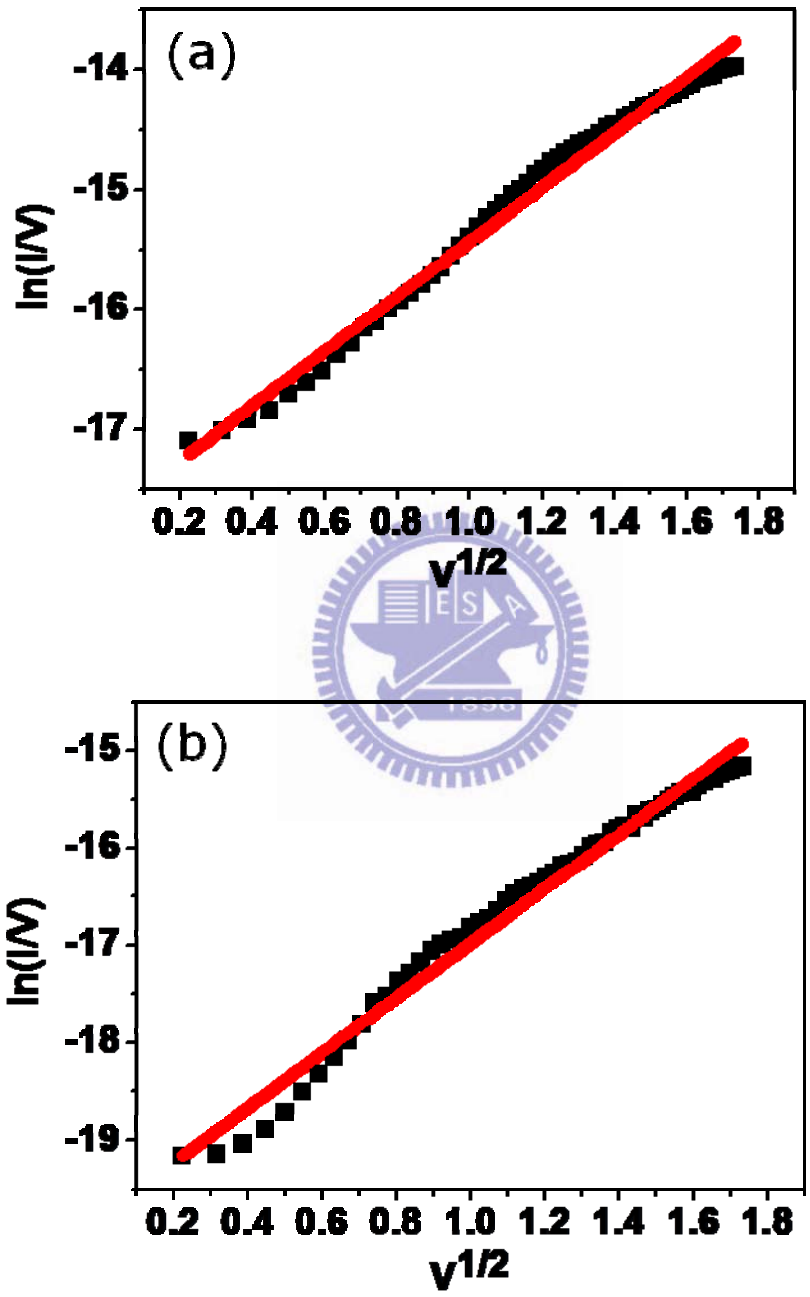

Fig. 4.3 : Curve fitting for (a) Si/LSRO (b) HSRO/LSRO multilayer structures with Poole-Frenkel emission model.

However, Poole-Frenkel emission model cannot explained the carrier transportation mechanism of Si NC thin films which are made of Si/SiO_2 and $HSRO/SiO_2$ multilayer structures, not shown here. In order to understand the carrier transportation mechanism of the two Si NC thin films, Schottky emission model is utilized to fit their I-V curves. Schottky emission model can be expressed by

$$I = A^{*}T^{2}\exp\left[-q(\Phi_B - \beta E^{\frac{1}{2}})kT\right] \quad (4.2)$$

Fig. 4.4 shows the fitting results. The I-V curves are well fitted by the Schottky model. Namely, carrier transportation of the two Si NC thin films dominates by carrier injection. From mention above, they support that LSRO barrier layer can provide additional transportation paths for carriers.

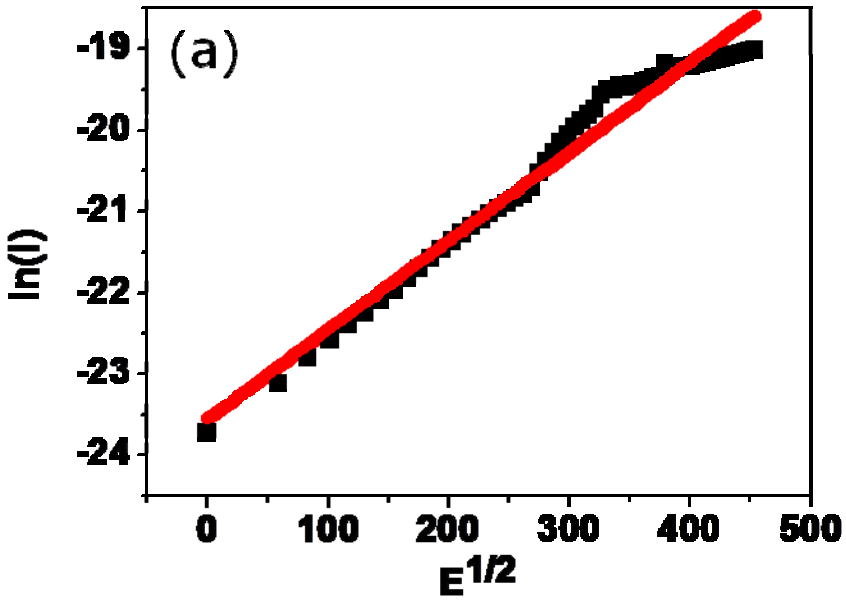

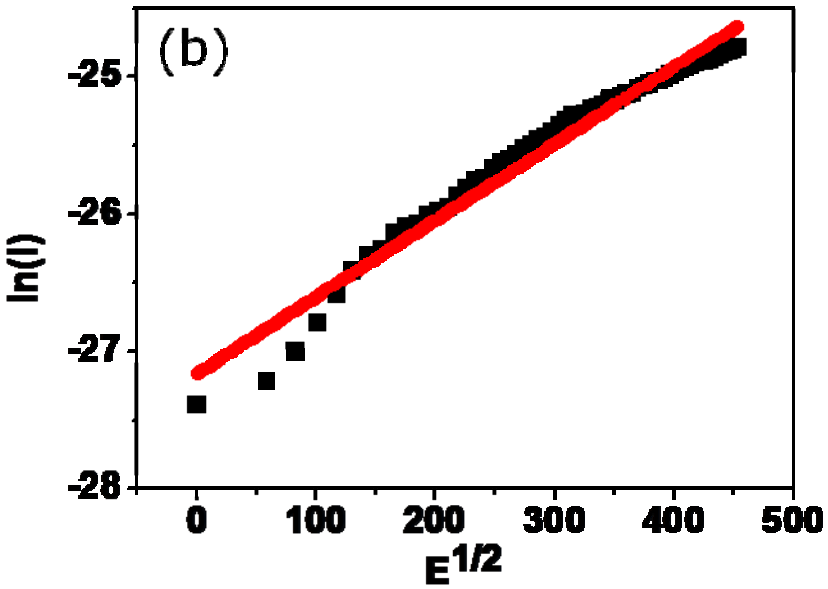

Fig. 4.4 : Curve fitting for (a) Si/SiO_2 (b) $HSRO/SiO_2$ multilayer structures with Schottky emission model.

4.3 Temperature Dependence I-V Curves of Si NC Thin Films

Hence, we estimate the barrier height of Si NC thin films using Si/LSRO and HSRO/LSRO multilayer structures by the measurements with temperature dependence I-V Curves. Poole-Frenkel emission model can be also expressed by

$$J_{PF} = q\,\mu\, n_t \times E \times \exp\left[\left(\frac{q}{kT}\sqrt{\frac{q}{\pi\varepsilon^2}} \times \sqrt{E} - \frac{q\Phi_t}{kT}\right)\right] \qquad (4.3)$$

where μ is the mobility, n_t is the defect density, Φ_t is the barrier high and T is the absolute temperature [23]. The barrier height which calculated according to equation (4.3) is 0.72eV and 0.88eV for Si NC thin films using Si/LSRO and HSRO/LSRO multilayer structures, respectively. Nenertheless, the barrier height is 3.2eV (from

lowest unoccupied molecule orbits) and 4.7eV (from highest occupied molecule orbits) for electrons and holes Si NC thin films with perfect SiO_2 barrier layers, respectively [24]. Although reduced barrier height may take influence on the quantum confinement effect of Si NC thin films when LSRO replaces SiO_2 as barrier layers, the quantum confinement effect of Si NC thin films is still observed in our case. As a result, barrier layers using LSRO can improve the conductivity of Si NC thin films, but make an ignorable influence on the quantum confinement effect.

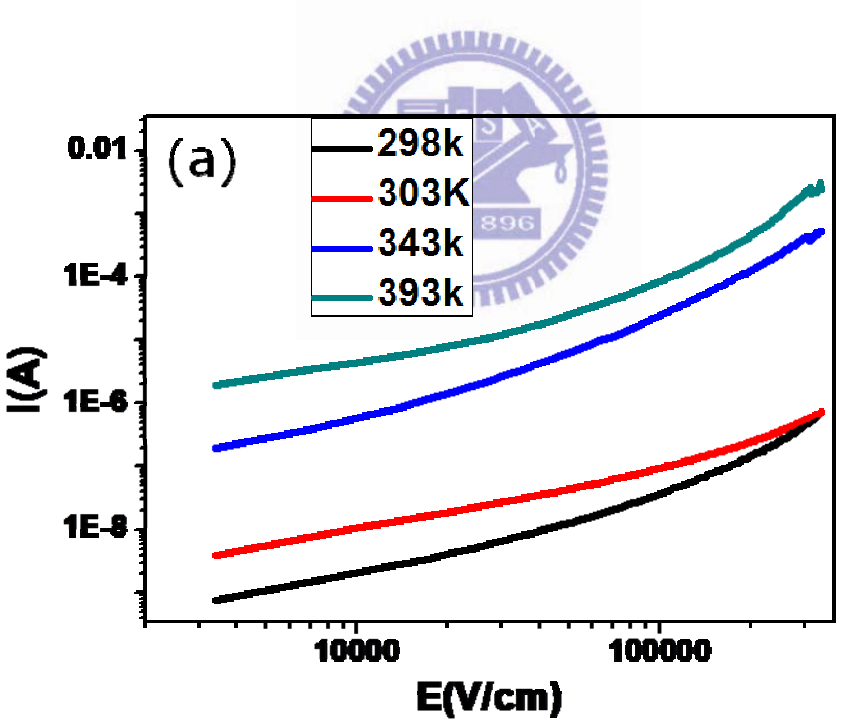

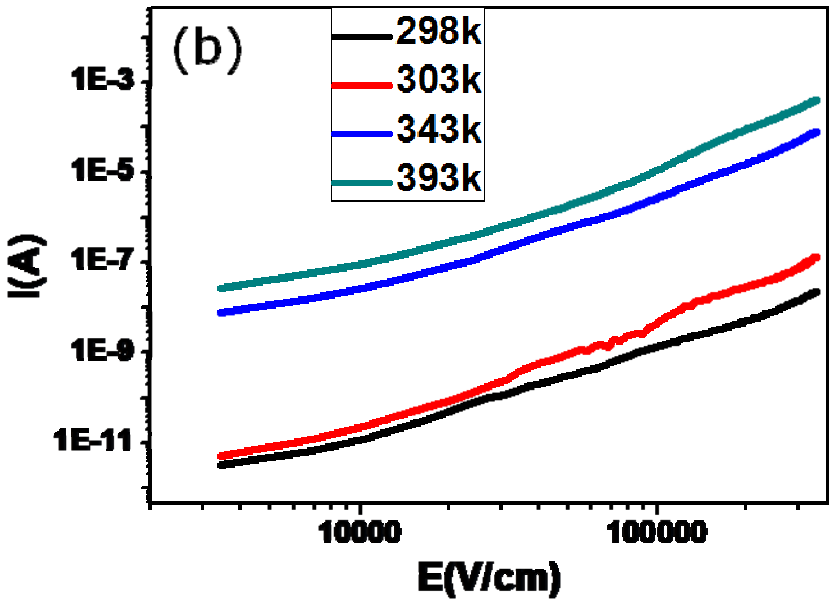

Fig. 4.5 : Temperature dependence for (a) Si/LSRO (b) HSRO/LSRO multilayer structures.

Chapter 5 Conclusion and Future Work

5.1 Conclusion

In this thesis, LSRO barrier layers are introduced to enhance carrier transportation. We deposited four 24 bilayers multilayer structures, including Si/SiO_2, HSRO/SiO_2, Si/LSRO and HSRO/LSRO, which the total thickness of thin films is 146 nm. In Raman spectra, we observe the crystallization of Si NC thin films and estimate the dimension of Si NC. the dimension of Si NC is also calculated by XRD analysis. The dimension is about 4~6 nm for Si NC thin films using Si as active layers and 2.5 nm for those using HSRO as active layers. The values are consistent with those estimated by Raman spectra. In PL spectra, a PL peak around 650 nm is defect states caused by LSRO barrier layers, which can offer additional transportation paths for carriers. I-V characteristics of Si NC thin films are improved when LSRO instead of SiO_2 as barrier layers is. The transportation mechanism of Si NC thin films using Si/SiO_2 and HSRO/SiO_2 multilayer structures dominates by Schottky emission, and that of Si NC thin films using Si/LSRO and HSRO/LSRO multilayer structures belongs to Poole-Frenkel emission. the barrier height of LSRO multilayer. Barrier heights are 0.72 eV and 0.88 eV for Si NC thin films using Si/LSRO and HSRO/LSRO multilayer structures, respectively. In spite of barrier height lowering which probably makes an impact on the quantum confinement effect of Si NC thin films, not only conductivity improvement of Si NC thin films but also the

quantum confinement effect of Si NC thin films are obtained in our cases.

5.2 Future Work

Even if Si NC thin films have been studied for decades, many issues still debate. The stress of Si NC thin films affects their crystallinity and dimension, which in turn makes influence on the Eg of Si NC thin films. We will change our annealing process such as laser annealing to reduce the stress effect. Because of amorphous phase of SiO_2 barrier layers, lots of the defects states can be found in the Si NC thin films. The nonradiative defect states can trap photogenerated carriers and thus degrade the performance of Si NC thin films. Many studies on the defect states have been published, but identification and origin of the defect states are not so clear so far. Here we observe an addition PL peak due to LSRO as barrier layers, which an indirect evidence of additional transportation paths for carriers but we still need a direct evident to proof our ideals. Thus we will pay much attention on identification and origin of three states observed in the PL spectra. Although the conductivity of Si NC thin films has been increased, it still high enough for photovoltaic applications. We can further increase the conductivity by impurity doping such B doping. It is expected that the performance of Si NC thin films will be further boosted by impurity doping such B doping, using other barrier materials such as SiN_x .

Reference

[1] J. Zhao, A. Wang, M.A. Green, F. Ferrazza, “19.8% efficient "honeycomb" textured multicrystalline and 24.4% monocrystalline silicon solar cells,” Appl. Phys. Lett. 73, 1991 (1998).

[2] M. A. Green, “Third generation photovoltaics: solar cells for 2020 and beyond,” Physica E, vol. 14, pp. 65-70, 2002.R. Hezel, Prog. PV Res. Appl. ,Vol.5, pp.109 (1997)

[3] Y. Kanemitsu, T. Ogawa, K. Shiraishi, and K. Takeda, “Visible PL from oxidized Si nanometer-sized spheres: Exciton confinement on a spherical shell,” Phys. Rev. B, vol. 48, pp. 4883- 4886, (1993)

[4] Eun-Chel Cho, Sangwook Park, Xiaojing Hao, Dengyuan Song1, Gavin Conibeer, Sang-Cheol Park and Martin A Green, "Silicon quantum dot/crystalline silicon solar cell,” Nanotechnology, vol. 19, pp. 245201, (2008)

[5] R. Rölver, B. Berghoff, D. Bätzner, B. Spangenberg, H. Kurz, M. Schmidt, B. Stegemann, “Si/SiO2 multiple quantum wells for all silicon tandem cells: Conductivity and photocurrent measurements,” Thin Solid Films, vol. 516, pp. 6736, (2008)

[6] B. Berghoff, S.Suckow, R. Rölver, B.Spangenberg, H.Kurz, A.Sologubenko, J.Mayer, “Quantum wellsbasedonSi/SiOx stacks fornanostructuredabsorbers,”

Solar Energy Materials & Solar Cells, article in press

[7] Green, M.A., Cho, E.-C., Cho, Y., Huang, Y., Pink, E., Trupke, T., Lin, A., "ALL-SILICON TANDEM CELLS BASED ON "ARTIFICIAL" SEMICONDUCTOR SYNTHESISED USING SILICON QUANTUM DOTS IN A DIELECTRIC MATRIX," 20th European Photovoltaic Solar Energy Conference, 6 – 10 June 2005, Barcelona, Spain

[8] R. Rölver, B. Berghoff, D. Bätzner, B. Spangenberg, H. Kurz, M. Schmidt, B. Stegemann, "Si/SiO2 multiple quantum wells for all silicon tandem cells: Conductivity and photocurrent measurements," Thin Solid Films, vol. 516, pp. 6736, (2008)

[9] B. Berghoff, S.Suckow, R. Rölver, B.Spangenberg, H.Kurz, A.Sologubenko, J.Mayer, "Quantum wells based on Si/SiOx stacks for nanostructured absorbers," Solar Energy Materials & Solar Cells, article in press

[10] X.J. Hao, E-C.Cho, C.Flynn, Y.S.Shen, S.C.Park, G.Conibeer, M.A.Green, "Synthesis and characterization of boron-doped Si quantum dots for all-Si quantum dot tandem solar cells," Solar Energy Materials & Solar Cells, Vol. 93, pp. 273–279, (2009)

[11] Gavin Conibeer, Martin Green, Richard Corkish, Young Cho, Eun-Chel Cho, Chu-Wei Jiang, Thipwan Fangsuwannarak, Edwin Pink, Yidan Huang, Tom Puzzer,

Thorsten Trupke, Bryce Richards, Avi Shalav, Kuo-lung Lin, Silicon nanostructures for third generation photovoltaic solar cells," Thin Solid Films, vol. 511 – 512, pp.654 – 662, (2006)

[12] C. V. Raman, and K. S. Krishna , " A new type of secondary radiation," Nature 121, 501 (1928).

[13] G. Faraci1,a, S. Gibilisco1, P. Russo1, A.R. Pennisi1, G. Compagnini2, S. Battiato2, R. Puglisi3, and S. La Rosa "Si/SiO2 core shell clusters probed by Raman spectroscopy" Eur. Phys. J. B 46, 457–461 (2005).

[14] S. Hernández, A. Martínez, P. Pellegrino, Y. Lebour, B. Garrido, E. Jordana, and J. M. Fedeli, "Silicon nanocluster crystallization in SiOx films studied by Raman Scattering," JOURNAL OF APPLIED PHYSICS 104, 044304, (2008)

[15] hipwan Fangsuwannarak, "Electronic and Optical Characterisations of Silicon Quantum Dots and its Applications in Solar Cells," University of New South Wales Sydney, Australia, (2007)

[16] X JHao, A P Podhorodecki, Y S Shen, G Zatryb, J Misiewicz and M A Green, "Effects of Si-rich oxide layer stoichiometry on the structural and optical properties of Si QD/SiO2 multilayer films," Nanotechnology, 20, 485703, (2009)

[17] Y. Kanemitsu, T. Ogawa, K. Shiraishi, and K. Takeda, "Visible PL from oxidized Si nanometer-sized spheres: Exciton confinement on a spherical shell," Phys. Rev.

B, vol. 48, pp. 4883- 4886, (1993).

[18] M. V. Wolkin, J. Jorne, P. M. Fauchet, G. Allan, and C. Delerue, “Electronic states and luminescence in porous silicon quantum dots: The role of oxygen,” Phys. Rev. Lett., vol. 82, pp. 197-200, (1999).

[19] J. S. Biteen, N. S. Lewis, H. A. Atwater, and A. Polman, “Size-dependent oxygen-related electronic states in silicon nanocrystals,” Appl. Phys. Lett., vol. 84, pp. 5389-5391, (2004).

[20] X. X. Wang, J. G. Zhang, L. Ding, B. W. Cheng, W. K. Ge, J. Z. Yu, and Q. M. Wang, “Origin and evolution of photoluminescence from Si nanocrystals embedded in a SiO2 matrix,” PHYSICAL REVIEW B 72, 195313, (2005)

[21] S. M. Sze, Physics of Semiconductor Devices, John Wiley & Sons, New York (1981).

[22] S. M. Sze, Physics of Semiconductor Devices, John Wiley & Sons, New York (1981).

[23] J. G. Simmons, “Generalized formula for the electric tunneling effect between silicon electrodes separated by a thin insulating film.” J. Appl. Phys, 34, No.6, (1963)

[24] B. Berghoffa, S.Suckow, R.R¨ olver, B.Spangenberg, H.Kurz, A.Sologubenko, J.Mayer, “Quantum wellsbasedonSi/SiOx stacks fornanostructuredabsorbers,”

article in press.